REPORT DOCUMENTATION PAGE

Form Approved OMB NO. 0704-0188

1. REPORT DATE (DD-MM-YYYY)	2. REPORT TYPE	3. DATES COVERED (From - To)
30-04-2019	Final Report	1-Jul-2016 - 31-Dec-2018

4. TITLE AND SUBTITLE
Final Report: Vertical Transport in InAs/GaSb and InAs/InAsSb Superlattices: 4.3 Electronic Sensing

5a. CONTRACT NUMBER
W911NF-16-2-0068

5b. GRANT NUMBER

5c. PROGRAM ELEMENT NUMBER
611102

6. AUTHORS

5d. PROJECT NUMBER

5e. TASK NUMBER

5f. WORK UNIT NUMBER

7. PERFORMING ORGANIZATION NAMES AND ADDRESSES
University of New Mexico Albuquerque
1700 Lomas Boulevard NE, Suite 2200, MSC01 1247
1 University of New Mexico
Albuquerque, NM 87131 -0001

8. PERFORMING ORGANIZATION REPORT NUMBER

9. SPONSORING/MONITORING AGENCY NAME(S) AND ADDRESS (ES)
U.S. Army Research Office
P.O. Box 12211
Research Triangle Park, NC 27709-2211

10. SPONSOR/MONITOR'S ACRONYM(S)
ARO

11. SPONSOR/MONITOR'S REPORT NUMBER(S)
69082-EL-H.1

12. DISTRIBUTION AVAILIBILITY STATEMENT
Approved for public release; distribution is unlimited.

13. SUPPLEMENTARY NOTES
The views, opinions and/or findings contained in this report are those of the author(s) and should not contrued as an official Department of the Army position, policy or decision, unless so designated by other documentation.

14. ABSTRACT

15. SUBJECT TERMS

16. SECURITY CLASSIFICATION OF:			17. LIMITATION OF ABSTRACT	15. NUMBER OF PAGES	19a. NAME OF RESPONSIBLE PERSON
a. REPORT	b. ABSTRACT	c. THIS PAGE			Sanjay Krishna
UU	UU	UU	UU		19b. TELEPHONE NUMBER 614-292-3715

RPPR Final Report
as of 01-May-2019

Agency Code:

Proposal Number: 69082ELH **Agreement Number: W911NF-16-2-0068**
INVESTIGATOR(S):

Name: Sanjay Krishna
Email: krishna.53@osu.edu
Phone Number: 6142923715
Principal: Y

Organization: **University of New Mexico Albuquerque**
Address: 1700 Lomas Boulevard NE, Suite 2200, MSC01 1247, Albuquerque, NM 871310001
Country: USA
DUNS Number: 868853094 EIN: 856000642

Report Date: 31-Mar-2019 Date Received: 30-Apr-2019
Final Report for Period Beginning 01-Jul-2016 and Ending 31-Dec-2018
Title: Vertical Transport in InAs/GaSb and InAs/InAsSb Superlattices: 4.3 Electronic Sensing
Begin Performance Period: 01-Jul-2016 **End Performance Period:** 31-Dec-2018
Report Term: 0-Other

Submitted By: Sanjay Krishna Email: krishna.53@osu.edu
Phone: (614) 292-3715

STEM Degrees: 2 **STEM Participants:** 2

Major Goals: Vertical transport in narrow band gap antimonide based type-II strained layer superlattices (T2SLs) is a significant problem for the design of Mid-Wave Infrared (MWIR, 3-5 ?m) photodetectors. Investigation of the transport of electrons and holes in T2SLs is necessary to understand better how or if one can improve carrier collection efficiency through design or changes in material properties of this essential infrared absorber material. This report provides lateral and vertical transport results using magneto-transport for InAsSb alloys (isotropic) and InAs/InAsSb T2SLs (anisotropic). Then, vertical transport using EBIC technique will be discussed with results for InAs/GaSb T2SL.

Accomplishments: Under the Army Research Office (ARO) funding, transport in InAsSb alloys and InAs/GaSb plus InAs/InAsSb T2SLs has been investigated theoretically and experimentally using magneto-transport (pertaining to alloy and InAs/InAsSb T2SL material) and Electron Beam Induced Current (EBIC) technique (pertaining to InAs/GaSb T2SL material). Lilian Casias has been responsible for the magneto-transport project in collaboration with the Air Force Research Laboratory (AFRL), Sandia National Laboratories (SNL) and Naval Research Laboratories (NRL). Zahra Taghipour has been responsible for the EBIC measurement performed at the Center for High Technology Materials (CHTM). In what follows, we summarize the progress in these projects, including test setups, growth, fabrication, characterization and experimental plus theoretical results.

Training Opportunities: Training and mentoring of Zahra Taghipour, Ph.D., and Lillian Cassias, Ph.D.

Professional development through conference presentations, journal article preparation and publication, thesis preparation and publication, and thesis defense.

Results Dissemination: "Carrier density and transport in Be-doped InAsSb for infrared detector materials", L. Casias, C. P. Morath, E. H. Steenbergen, P. Webster, J. Kim, V. Cowan, G. Balakrishnan, and S. Krishna, MIOMD, October 2018, Poster Presentation.

Casias, Lilian K., et al. "Carrier concentration and transport in Be-doped InAsSb for infrared sensing applications." SPIE Conference Series. Vol. 10624. 2018.

Casias, Lilian K., et al. "Carrier concentration and transport in Be-doped InAsSb for infrared sensing applications." Infrared Physics & Technology 96 (2019): 184-191.

Z. Taghipour et al., "Temperature-Dependent Minority-Carrier Mobility in p -Type InAs / GaSb Type-II Superlattice Photodetectors," Phys. Rev. Appl., vol. 11, no. 024047, 2019.

DISSERTATIONS
Vertical Transport Study of III-V Type-II Superlattices, Zahra Taghipour, University of New Mexico, December 2018.

Transport in Mid-Wavelength Infrared (MWIR) p- and n- type InAsSb and InAs/InAsSb Type-II Strained Layer Superlattices (T2SLs) for infrared detection, Lilian K. Casias, University of New Mexico, May 2019

Honors and Awards: Nothing to Report

Protocol Activity Status:

Technology Transfer: Nothing to Report

PARTICIPANTS:

Participant Type: Graduate Student (research assistant)
Participant: Lilian Casias
Person Months Worked: 12.00 **Funding Support:**
Project Contribution:
International Collaboration:
International Travel:
National Academy Member: N
Other Collaborators:

Participant Type: Graduate Student (research assistant)
Participant: Zahra Taghipour
Person Months Worked: 12.00 **Funding Support:**
Project Contribution:
International Collaboration:
International Travel:
National Academy Member: N
Other Collaborators:

Participant Type: Co PD/PI
Participant: Ganesh Balakrishnan
Person Months Worked: 1.00 **Funding Support:**
Project Contribution:
International Collaboration:
International Travel:
National Academy Member: N
Other Collaborators:

RPPR Final Report
as of 01-May-2019

UNIVERSITY OF NEW MEXICO

PROGRESS REPORT
Award Number: W911NF-16-2-0068

Transport in InAsSb alloys, InAs/InAsSb and InAs/GaSb Type-II Strained Layered Superlattices (T2SL)

Authors:
Lilian Casias,
Zahra Taghipour

PI:
Prof. Sanjay Krishna/Prof. Ganesh Balakrishnan

April 2019

Contents

I. Introduction

Interest in II-VI materials such as Mercury Cadmium Telluride (MCT) and III-V semiconductor materials (such as InSb, InAsSb and Type-II Strained Layer Superlattices (T2SLs)) has been ongoing through many years for infrared detector applications. III-V antimonide (Sb) based materials, such as $InAs_{0.91}Sb_{0.09}$ alloy absorber layers lattice matched to a GaSb substrate can be an alternative to MCT detectors in the MWIR 3-5 μm wavelength range [1], [2]. Antimonide based Type-II Strained Layer Superlattices (T2SLs) have gained significant attention and were first proposed in the late 70s and 80s by Esaki and other researchers [3], [4]. Carrier lifetime while being an important material parameter for detectors, does not solely determine their performance. Once charge is generated in a detector, it must be effectively extracted from the device as photocurrent. Hence, understanding carrier transport parameters is therefore fundamentally important in advancing III-V IR photodetectors. Carrier transport vertically (parallel to the growth axis or growth direction) through the material is of special interest because carrier conduction via this path is the typical mode of operation for infrared detectors and it affects the collection efficiency of the detector.

Transport studies on III-V IR materials have been the subject of continued research [5]–[10] and it is the topic of interest of this report. To fully understand the transport in III-V materials, in-plane or lateral transport measurements need to be better understood. In-plane transport properties are usually extracted using Hall Effect measurements and can be difficult to perform in InAsSb and InAs/InAsSb T2SLs due to the parallel conduction in the highly conductive GaSb substrate as well as surface electron accumulation layers. Although there is a rapid progress of III-V detector technology, transport remains a limiting factor for the material. Further development demands a better understanding of lateral (in-plane) and vertical (out-of-plane) carrier transport mechanisms and extraction of all the carrier species responsible for conduction.

Under the Army Research Office (ARO) funding, transport in InAsSb alloys and InAs/GaSb plus InAs/InAsSb T2SLs has been investigated theoretically and experimentally using magneto-transport (pertaining to alloy and InAs/InAsSb T2SL material) and Electron Beam Induced Current (EBIC) technique (pertaining to InAs/GaSb T2SL material). Lilian Casias has been responsible for the magneto-transport project in collaboration with the Air Force Research Laboratory (AFRL), Sandia National Laboratories (SNL) and Naval Research Laboratories (NRL). Zahra Taghipour has been responsible for the EBIC measurement performed at the Center for High Technology Materials (CHTM). In what follows, we summarize the progress in these projects, including test setups, growth, fabrication, characterization and experimental plus theoretical results.

II. Overall objective of the effort

Vertical transport in narrow band gap antimonide based type-II strained layer superlattices (T2SLs) is a significant problem for the design of Mid-Wave Infrared (MWIR, 3-5 μm) photodetectors. Investigation of the transport of electrons and holes in T2SLs is necessary to understand better how or if one can improve carrier collection efficiency through design or changes in material properties of this essential infrared absorber material. This report provides lateral and vertical transport results using magneto-transport for InAsSb alloys (isotropic) and InAs/InAsSb T2SLs (anisotropic). Then, vertical transport using EBIC technique will be discussed with results for InAs/GaSb T2SL.

III. Significant Accomplishments

1. Magneto-Transport

1.1 Multi-Carrier Transport with Variable Magnetic Field

Multi-carrier conduction results because the carrier charge, mobility, and energy of the carriers, and their interaction with the host material is different for various energy bands (multi-band) or for various conduction paths (multi-layers) in multi-layered structures. Information provided by the Hall Effect measurement at a single field and at one temperature, will only provide the average mobility and carrier concentration of all carriers which will not be reliable information for a multi-carrier system. Thus, variable temperature- and magnetic-field-dependent transport measurements must be employed. If the variable magnetic-field Hall Effect technique is employed at different temperatures, information on the freeze-out of carriers and scattering mechanisms can also be obtained. Hence, magneto-transport experiments as a function of the magnetic field are needed to provide more information in such systems for each carrier type. The concept of Magneto-Transport (MT) was first introduced in 1956 [11]. An MT measurement is very well described by its name, where one can record the resistance of the material as different magnetic fields are applied.

1.2 Methods

The Hall Effect measurement equipment used for this work was the LakeShore Cryotronics Model 9509 Hall Measurement System (HMS) equipped with a 9-Tesla superconducting magnet. The HMS setup is located at Kirtland Air Force Research Laboratory (AFRL) and is shown in Figure 1.

Figure 1: LakeShore Cryotronics Hall Measurement System, (a) Model 9509 cryogenic dewar with sample insert mounted in the dewar, (b) electronics equipment rack.

The Hall measurement settings used for this work contain 52 magnetic field values from -9-T to 9-T and temperatures ranging from 15 K to 390 K as it was shown to be the standard used at the University of Western Australia (UWA). In addition, two types of electrical configurations were used for lateral (Figure 2) and vertical measurements (Figure 3).

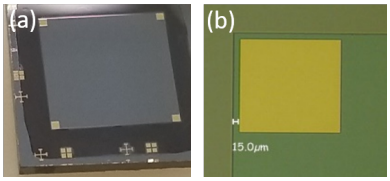

Figure 2: (a) van Der Pauw (VDP) patterned *n*-type InAs/InAsSb 5 mm x 5 mm sample with four 300 µm ohmic contacts placed on the perimeter of the sample and aligned using the alignment marks, (b) Microscope picture showing the 15 µm offset at one of the four corners. Offsets of 15 or 25 µm are an option in the mask to account for any wet etching uniformities of the mesa sidewalls.

Since the Hall Effect technique is not applicable for vertical transport measurements, a geometrical magneto-resistance approach is used for vertical transport measurements instead. Like lateral measurements, the samples used for vertical transport measurements are also mounted onto a sample carrier and wirebonded. However, unlike the lateral measurement that only contains four contacts (VDP geometry) on the top of the sample, the vertical configuration uses a top and bottom contact as shown in Figure 3.

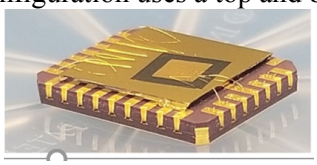
Figure 3: Vertical transport sample with top contact and sapphire coated with Ti/Pt/Au which acts as the bottom contact, sample is mounted on a non-magnetic chip carrier (LCC02861)

NRL MULTIBANDS® software was used to obtain band-diagrams plus estimate carrier concentration build-up at the interfaces. Secondly, Multiple-Carrier Fit (MCF) was used and High-Resolution Mobility Spectrum Analysis (HR-MSA) the different carriers contributing to lateral and vertical conduction, respectively.

1.3 Goal of the Magneto-Transport Study

The goal of the magneto-transport measurements are: (1) study the lateral/vertical transport of electrons and holes in MWIR InAsSb and InAs/InAsSb T2SLs, and (2) to extract vertical transport mobilities in InAs/InAsSb T2SL using a Metal-Semiconductor-Metal (MSM) processing method. In order to accomplish such goals, the work was divided into three steps as shown in Figure 4.

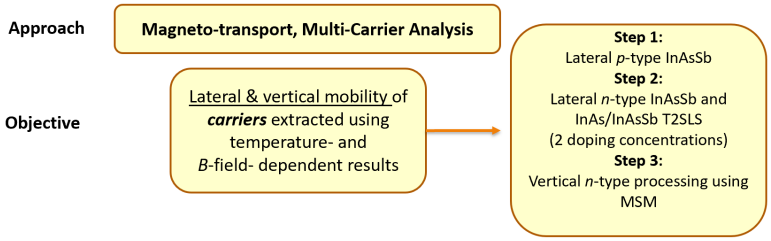

Figure 4: Approach and objective of the work presented in the magneto-transport work which involves three steps.

Step 1 incorporated a theoretical and experimental investigation of lateral transport in MWIR *p*-type InAsSb. Step 2 followed a similar method, but the lateral measurements are performed on *n*-type InAsSb and InAs/InAsSb T2SLs detectors. As mentioned previously, lateral transport measurements were performed in order to better understand the different conduction paths present in the material. Step 3 proposed a different processing method, the MSM, and measures magneto-resistance in *n*-type InAs/InAsSb T2SLs detectors, while extracting the vertical transport mobility in T2SL. The process and the results of the steps taken for this work are explained in the next sections.

1.4 Step 1: InAsSb *p*-type Lateral Transport

For this study, the sample was grown on an *n*-type (*Te*-doped) GaSb substrate using Molecular Beam Epitaxy (MBE). The structure is shown in Figure 5 (a), which consists of a 2 µm thick lattice-matched $InAs_{0.91}Sb_{0.09}$ bulk layer with a target *p*-type Be-doping concentration of 2×10^{18} cm^{-3} grown on top of a 0.01 µm thick undoped GaSb buffer layer on a 0.5 µm thick lattice-matched and undoped (*NID*) $AlAs_{0.08}Sb_{0.92}$ insulating layer. The 2-dimensional and 3-dimensional fabricated sample diagrams are shown in Figure 5 (a) and (b) with van der Pauw (VDP) configuration.

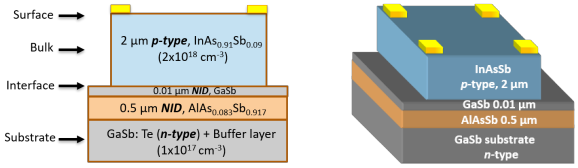

(a) **(b)**

Figure 5: Schematics of the fabricated samples in van der Pauw (VDP) configuration: (a) 2-dimensional InAsSb sample cross section with distinct conductive paths indicated (b) 3-dimensional etched InAsSb sample structure.

To attribute each carrier species suggested by MCF with a corresponding physical conduction process of the InAsSb samples at 77 K and 300 K, the samples were etched to different thicknesses and variable-field measurements were utilized to assist in confirming whether a carrier species represents bulk, interface or surface conduction. Then, a surface treatment experiment was conducted to correlate one of the electron conducting populations with conducting electrons at the surface of the mesa. The concentrations of two interface carriers were compared to the experimental data using the NRL MULTIBANDS® model. Variable temperature measurements (15 – 390 K) enabled the confirmation of the different carrier species and resulted in further extraction of bulk hole carrier and surface electron transport properties as a function of temperature. Like the results at 77 K, MCF also extracted four carrier populations at 300 K: a high-conductivity hole population (*h1*), a secondary hole population (*h2*) with higher mobility than *h1*, and two electron populations (*e1* and *e2*). As shown in Figure 6 (a) and (b), the *h2* carrier showed non-monotonic behavior.

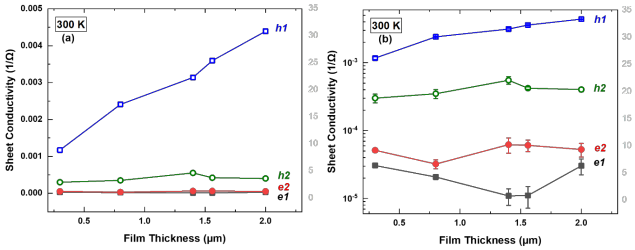

Figure 6: The average conductivity of the four carrier populations present in the *p*-type InAsSb structure at 300 K as a function of etched thickness on a (a) linear scale and (b) semilog scale with error bars.

The primary hole conductivity was confirmed to be that of the bulk hole in InAsSb. The bulk hole concentrations and mobilities at 77 K (300 K) are 1.6×10^{18} cm^{-3} (2.3×10^{18} cm^{-3}) and 125 cm^2 V^{-1} s^{-1} (60 cm^2 V^{-1} s^{-1}) indicating that the Be dopants are 100% ionized at room temperature and are 70% ionized at 77 K. A surface treatment experiment was conducted and correlated one of the electron conducting populations to the surface. The two remaining carriers are native to the InAsSb/GaSb/AlAsSb interface, as the experimentally measured sheet charge concentrations are consistent with the carrier concentrations modeled using the NRL MULTIBANDS® model. Variable temperature (15 – 390 K) measurements confirmed the different carrier species present in the sample and enabled the extraction of the bulk hole, interface carriers and surface electron transport properties. For the bulk carrier, a thermal activation of intrinsic carriers at high temperatures (320 – 390 K) with a bandgap of $E_G \sim 258$ meV was found, which was comparable to

the modeled room temperature $InAs_{0.91}Sb_{0.09}$ bandgap of ~270 meV. In addition, the low temperature slope suggested a Be doping activation energy of $E_A \sim 22$ meV. Temperature analysis confirmed a surface carrier electron with resulting mobilities and sheet concentrations at 30 K (300 K) of 4500 $cm^2\ V^{-1}\ s^{-1}$ (4300 ± 100 $cm^2\ V^{-1}\ s^{-1}$) and 5.6×10^{10} cm^{-2} ($6\times10^{10} \pm 2\times10^{10}$ cm^{-2}), respectively. The work in this step was published and further details can be found in this reference: [12].

1.5 Step 2: *n*-type InAsSb and InAs/InAsSb Type-II Strained Layered Superlattices (T2SLs) Lateral Transport

For the step presented here, four samples were grown on an *n*-type (*Te*-doped) GaSb substrates using MBE. Each pair of structures are shown in Figure 7 (a) and (b), where each structure is shown with two doping concentrations. Figure 7 (a) consist of a 2 µm thick lattice-matched $InAs_{0.91}Sb_{0.09}$ bulk layer with undoped (*NID* or *n*-type 1×10^{15} cm^{-3}) and with an *n*-type Silicon-doping concentration of 1×10^{16} cm^{-3}.

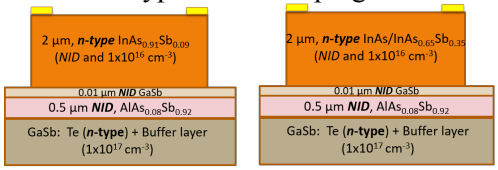

(a) **(b)**

Figure 7: Schematics of the fabricated *n*-type samples in van der Pauw (VDP) configuration, (a) 2-dimensional InAsSb sample cross section (b) 2-dimensional InAs/InAsSb T2SL sample cross section with two doping concentrations (*NID* and 1×10^{16} cm^{-3}).

A comparison of the bulk carrier between alloys and superlattices to provide further insight into the lateral transport properties was presented. The lateral bulk electron mobilities found for the alloy and superlattice samples is shown in Figure 8 for both doping concentrations, while Figure 8 (b) and (c) display the *NID* and Silicon-doped results with single-field mobility values at 77 and 300 K for a magnetic field (*B*) of 0.5T, respectively.

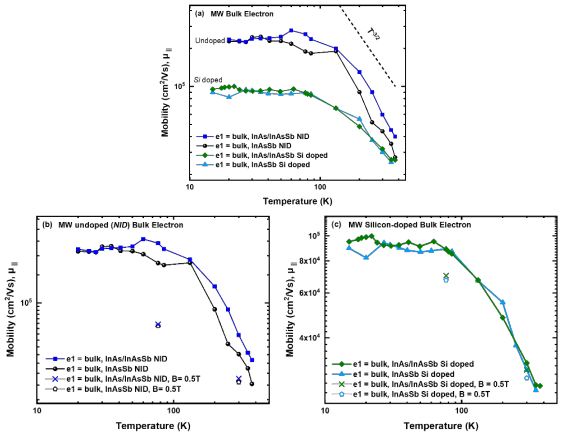

Figure 8: Lateral bulk electron mobilities vs. temperature for (a) undoped (*NID*) and Silicon-doped InAsSb alloys and InAs/InAsSb T2SL samples while (b) and (c) display the *NID* and Silicon-doped results with single-field mobility values at 77 and 300 K for a magnetic field (*B*) of 0.5T, respectively. Reference guidelines have been added to the mobility plot ($T^{-3/2}$) to represent lattice (phonon) scattering.

In this step, similar magnitude and temperature dependence of the bulk electron mobilities and concentrations are found for MWIR InAsSb alloys and InAs/InAsSb T2SL samples as a function of doping (*NID* to Si-doped). A surface treatment experiment was conducted and correlated one of the electron conducting populations to the surface. The interface carriers are linked to the InAsSb/GaSb/AlAsSb or T2SL/GaSb/AlAsSb interface, as the experimentally measured sheet concentrations are consistent with the

carrier concentrations modeled using the NRL MULTIBANDS® model at 300 K. Transport properties extracted for the *n*-type InAsSb alloys and the InAs/InAsSb T2SLs are summarized in Tables 5.5-5.8 and Tables 5.9-5.12 under 77 and 300 K, respectively in Lilian Casias Dissertation at UNM, May 2019 (Publication reference at the end of the Report). The lateral transport results should prove of assistance for vertical transport measurements as a comparison to lateral transport properties for isotropic (InAsSb) and anisotropic (InAs/InAsSb T2SLs) materials. Conventional transport measurements such as variable-field Hall effect measurements can suffice for lateral transport diagnostics, however vertical transport is a much more challenging task that is reported in Step 3.

1.6 Step 3: *n*-type InAs/InAsSb Type-II Strained Layered Superlattice (T2SL) Vertical Transport

It has been shown in Step 1(*p*-type $InAs_{0.91}Sb_{0.09}$) and Step 2 that by performing lateral Hall Effect and resistivity measurements over a range of temperature and magnetic fields, it is possible to separate contributions from different carrier species using a MCF analysis. This step proposed a different processing technique to measure vertical transport properties on the same *n*-type T2SL absorber materials ($InAs/InAs_{0.65}Sb_{0.35}$). Hence, substrate-removed, Metal-Semiconductor-Metal (MSM) devices were fabricated to attempt vertical transport measurements for the first time on such material. The MSM fabrication allows for geometrical magneto-resistance (MR) measurements on superlattice structures after the GaSb substrate and etch stop layers have been mechanically and chemically removed, with the purpose that only the carriers from the absorber materials are considered. In this work, for the first time, MSM processing to extract vertical transport measurements of T2SL anisotropic materials. For this vertical transport study, two ($n^+n^-n^+$) samples were grown on an *n*-type (*Te*-doped) GaSb substrates using MBE. The structure is shown in Figure 9, where two doping concentrations for the absorber layer are used: (1) 1×10^{15} cm^{-3} or non-intentionally doped (*NID)* and (2) 1×10^{16} cm^{-3} Silicon-doped (Si-doped). The structures consist of a 2 µm thick lattice-matched $InAs/InAs_{0.65}Sb_{0.35}$ T2SL absorber layer.

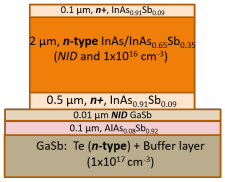

Figure 9: Cross-section of the MBE grown ($n^+n^-n^+$) $InAs/InAs_{0.65}Sb_{0.35}$ T2SL samples. The structure is shown with two doping concentrations for the absorber layer: (1) 1×10^{15} cm^{-3} or non-intentionally doped (*NID)* and (2) 1×10^{16} cm^{-3} Silicon-doped (Si-doped).

In order to fabricate the MSM structure, the 2 µm superlattice absorber layers must be isolated from the growth substrate, processing of the top and bottom contacts, and transfer to a non-conductive substrate must occur. Upon growth, the pieces of the wafer are diced into squares of 8 mm x 8 mm for easy handling and for a more uniform etching. The steps for the MSM structure are in Figure 10.

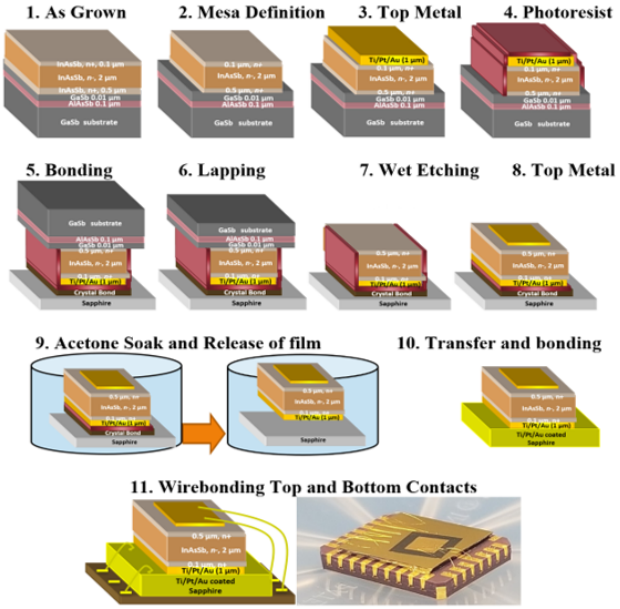

Figure 10: Schematic of the fabrication steps used for the Metal-Semiconductor-Metal (MSM) structure used for vertical transport measurements. Details for each step are provided in Sections 6.4.3.1 - 6.4.3.7.

After fabrication, there were four resistance configurations used in this work, Figure 11 illustrates the four-wire experimental setup with applied electric field (*E field*) and magnetic field (*B field*). Figure 11 (a) demonstrates the 3-dimensional and (b) the 2-dimensional four-wire setup used on the MSM structures. As seen in Figure 11 (b) the top contacts are classified as 1 and 2, while bottom contacts are 3 and 4. The magneto-resistance setup will measure the sheet resistance (R_s) as a function of magnetic field. For this work, the experimental data was obtained by measuring resistance (R) using top (1,2) and bottom (3,4) contact configurations as illustrated in Figures 11 (a) and (b). The four resistance configurations ($R_{I+I-V+V-}$) when applying a 700 µA current and sensing the voltage are: R_{1324}, R_{1423}, R_{2314}, R_{2413}.

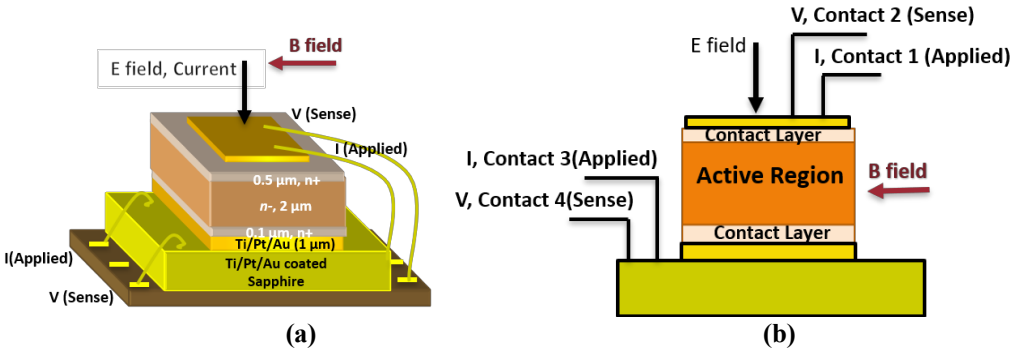

Figure 11: Experimental setup used with applied electric field (*E field*) and magnetic field (*B field*), (a) demonstrates the 3-dimensional and (b) the 2-dimensional four-wire setup used on the MSM structures. The top contacts are classified as 1 and 2, while bottom contacts are 3 and 4.

Figures 12 (a) and (b) illustrates the testing configuration used for magneto-transport measurements.

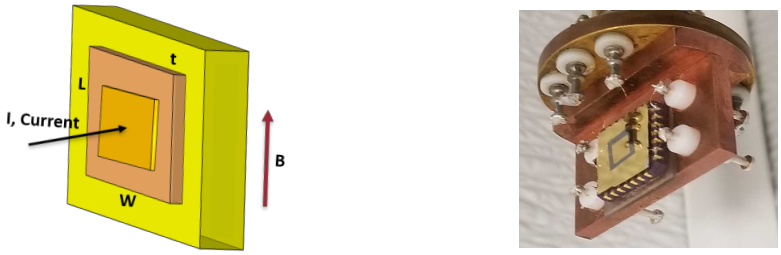

(a) **(b)**

Figure 12: Testing configurations used with (a) applied current I (*E field*) and magnetic field (*B field*); where w, t and L are the width, thickness and length of the sample under test and (b) a picture of the sample mounted for testing.

Hence, since single-carrier analysis could not be employed, the measured magneto-resistance characteristics were analyzed using HR-MSA as a collaborative effort with UWA. Using HR-MSA, the measured sheet resistance (R_s(B)) gets converted to longitudinal conductivity tensor component (σ_{xx}) that assumes the presence of N distinct carriers:

$$\sigma_{xx}(B) = \frac{1}{R_s(B)} = \sum_{i=1}^{N} \frac{q n_i \mu_i}{1+(\mu_i B)^2} \quad (1)$$

where R_s(B) is the measured sheet resistance as a function of magnetic field, q is electron charge, and n_i, μ_i are the electron concentration and mobility values for the i_{th} carrier [13]–[15]. The $(n^+n^-n^+)$ MSM fabricated devices contain an InAs/InAs$_{0.65}$Sb$_{0.35}$ T2SL anisotropic narrow gap absorber with two different doping concentrations. Magneto-resistance measurements were utilized to demonstrate multi-carrier conduction in the samples. Figure 13 illustrates the experimentally measured resistance versus magnetic field (B) for *NID* InAs/InAsSb T2SL sample at temperatures (a) 20, (b) 50, and (c) 130 K.

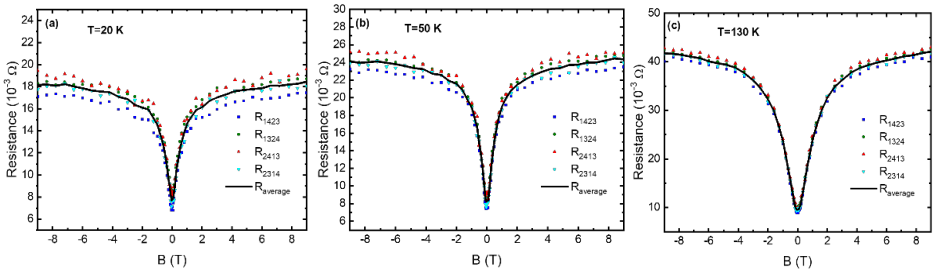

Figure 13: Resistance versus magnetic field (B) results for non-intentionally doped (*NID)* InAs/InAsSb T2SL sample at temperatures (a) 20, (b) 50, and (c) 130 K under four resistance configurations, with the average resistance of the configurations displayed as a solid line.

Under variable-temperature, the non-linear resistance behavior of all four resistance configurations with respect to B indicate multiple-carrier species (conduction paths. The *NID* InAs/InAs$_{0.65}$Sb$_{0.35}$ T2SL results were analyzed using HR-MSA at UWA. Figure 14 illustrates the sheet conductance versus magnetic field (B) for the average magneto-resistance dataset and the HR-MSA fit at (a) 20, (b) 77 and (c) 300 K. Analysis of the longitudinal conductivity tensor ($\sigma_{xx}(B)$) or sheet conductance is done using Equation 1.

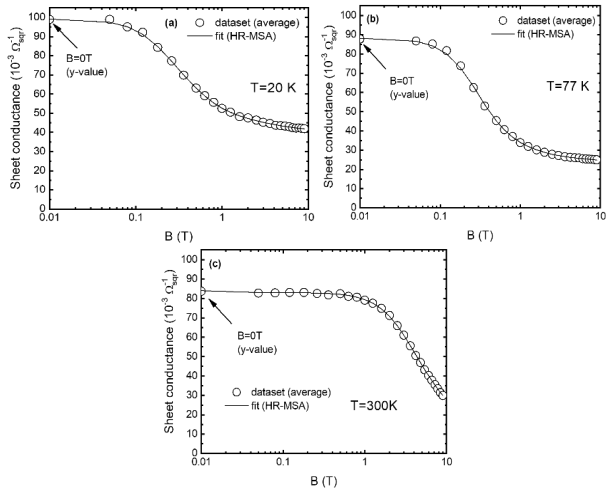

Figure 14: Sheet conductance for *NID* InAs/InAsSb T2SL versus magnetic field (*B*) for the average magneto-resistance dataset and the HR-MSA fit for (a) 20, (b) 77 and (c) 300 K.

Finally, the mobility spectrum for selected temperatures from 20 to 350 K using HR-MSA is shown in Figure 15. High mobility/conductance carrier is assigned to an electron and low mobility/conductance carrier to a hole. As mentioned, SNR is worse at low temperatures, leading to possible noise related artifacts in the spectra (additional peak).

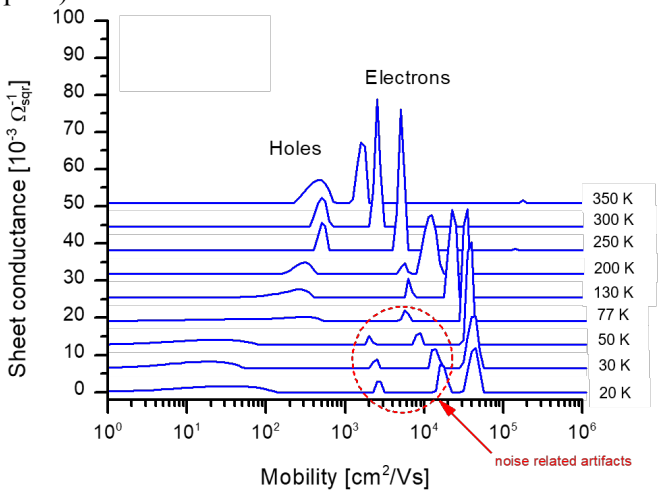

Figure 15: Mobility spectrum result for the *NID* InAs/InAsSb T2SL sample at selected temperatures from 20 to 350 K using HR-MSA. High mobility/conductance carrier is assigned to an electron and low mobility/conductance to a hole. SNR is worse at low temperatures, leading to possible noise related artifacts in the spectra.

As shown in Figure 15, a vertical electron (high mobility/conductance) and a hole (low mobility/conductance) are identified. Without properly decoupling the vertical mobility, an average of the lateral and vertical mobilities is extracted (coupled results). Hence, using the lateral mobility versus temperature results extracted in Step 2 for the *NID* InAs/InAsSb T2SL sample. Figure 16 illustrates the lateral, coupled vertical and decoupled vertical electron mobility results for the *NID* InAs/InAsSb T2SL sample.

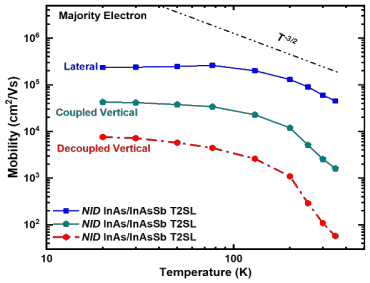

Figure 16: Majority electron comparison for lateral ($\mu_{||measured}$), coupled vertical ($\mu_{\perp coupled}$), and decoupled vertical ($\mu_{decoupled}$) results of mobility versus temperature for the *NID* InAs/InAsSb T2SL sample. Reference guideline has been added to the mobility plot to represent lattice scattering behavior ($T^{-3/2}$).

In Figure 16, lateral electron mobility is larger than the decoupled vertical electron mobility. Unlike lateral mobility, the carriers experience the presence of the nanometer scale and periodic potential wells along the vertical direction, thus, larger lateral mobility is expected in such anisotropic T2SL sample. At 77 K, the calculated decoupled vertical electron mobility is found to be 4.4×10^3 cm^2/Vs using the lateral electron mobility of 2.6×10^5 cm^2/Vs (lateral results found in Step 2) for the NID InAs/InAsSb T2SL. Figure 17 illustrates the lateral, coupled vertical and decoupled vertical hole mobility versus temperature (T) results for the *NID* InAs/InAsSb T2SL sample, and (b) plots the mobility versus temperature ($1/k_BT$) of the vertical hole minority carrier, where k_B is the Boltzmann constant (8.62×10^{-5} eV/K). Referring to Figure 17 (a), the lateral hole mobility shows lattice scattering dependence at high temperatures.

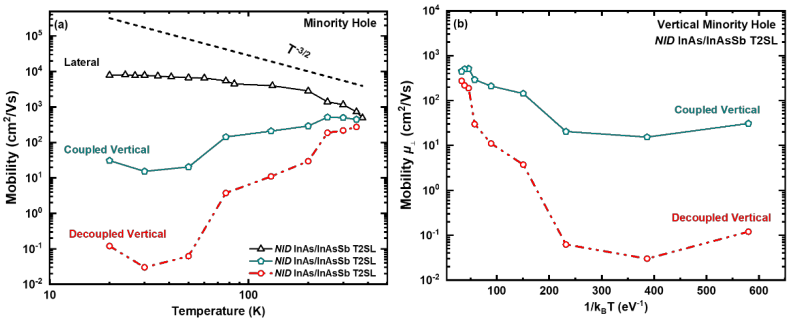

Figure 17: (a) illustrates the lateral, coupled vertical and decoupled vertical hole mobility versus temperature (T) results for the *NID* InAs/InAsSb T2SL sample, and (b) plots the mobility versus temperature ($1/k_BT$) of the vertical hole minority carrier, where k_B is the Boltzmann constant (8.62×10^{-5} eV/K). Reference guideline has been added to the mobility plot to represent lattice scattering behavior ($T^{-3/2}$).

In Figures 17 (a) and (b), it appears that vertical hole mobility (decoupled) is primarily affected by localization/hopping at low temperatures, Olson *et al.* [16] reported a similar vertical hole mobility trend in the *NID* *n*-type InAs/$InAs_{0.55}Sb_{0.45}$ T2SL using Heterojunction Bipolar Transistors (HBTs) and Photoluminescence (PL) measurements. Their results indicated carrier localization to play a critical role in the vertical hole transport and suggested the presence of defect level through which hopping transport occurs [16]. Therefore, the mobility trend and low-mobility values suggest that this carrier is the intrinsic minority vertical hole. Extracted from Step 2 results, the lateral hole mobilities were found at 77 K (300 K) are 5450 cm^2/Vs (1160 cm^2/Vs), while the measured coupled vertical hole mobilities found using HR-MSA in this study are 77 K (300 K) are 143 cm^2/Vs (501 cm^2/Vs) for the *NID* InAs/$InAs_{0.65}Sb_{0.35}$ T2SL. Then, decoupling the vertical mobility, the decoupled vertical hole mobilities found in this study are 77 K (300 K) are 3.73 cm^2/Vs (216 cm^2/Vs). For InAs/InAsSb T2SLs at 77 K, the lateral hole mobility results closely agree with the work reported by Brown *et. al* [17] using magneto-transport and MSA, while the vertical hole mobility results agree with work reported by Yon *et al.* [18] using Electron Beam Induced Current

(EBIC) and Time-Resolved Photoluminescence (TRPL). The extracted decoupled vertical hole mobilities reported in this work can be of benefit for the *n*B*n* InAs/InAsSb T2SL photodetector community, as this devices rely primarily on hole transport for operation. Finally, Table 1 chronologically summarizes the vertical transport mobility results reported for III-V material (InAsSb alloy, InAs/GaSb and InAs/InAsSb T2SLs) using different methods with the added contribution from the work presented in this report for the MSM processed magneto-resistance superlattice at 77 and 130 K. In Table 1, μ_e and μ_h are the vertical $(\mu_\perp)$ electron and hole mobilities, respectively. Reference information is provided for each study if the reader wants to investigate specific results and details.

Table 1: Chronological summary of the vertical transport mobility results reported for III-V material (InAsSb alloy, InAs/GaSb and InAs/InAsSb T2SLs) using different methods with the added contribution from the work presented in this dissertation for the MSM processed magneto-resistance InAs/InAsSb T2SL at 77 and 130 K. Symbols μ_e and μ_h are the vertical $(\mu_\perp)$ electron and hole mobilities, respectively. Reference information is provided for each study.

Method	Material	Vertical $\mu_\perp$ (cm^2/Vs)	Temperature (K)	Ref., Year
Cyclotron Resonance	MWIR *p*-type InAs/GaSb	$\mu_e = 7.6\times10^3$	4	[19],
	LWIR *p*-type InAs/GaSb	$\mu_e = 1.5\times10^4$	4	2011
Magneto-Resistance	LWIR *p*-type InAs/GaSb	$\mu_h = 280 \pm 27$	80-150	[20],
		$\mu_e = 2.4\times10^3 \pm 75$	80-150	2012
TRDT	MWIR *n*- & *p*-type InAs/GaSb	$\mu_e = 700 \pm 80$	77	[21],
		$\mu_h = 6 \pm 5$		2013
Transient Response	LWIR *n*-type $InAs_{0.60}Sb_{0.40}$	$\mu_h = 800$	77	[22], 2014
EBIC/TRPL	MWIR *n*B*n* InAs/$InAs_{0.81}Sb_{0.19}$	$\mu_h = 60$	6	[9], 2015
EBIC/TRPL	MWIR *n*B*n* InAs/$InAs_{0.65}Sb_{0.35}$	$\mu_h = 4$	80	[18] 2017
HBT/PL	MWIR *NID n*-type InAs/$InAs_{0.55}Sb_{0.45}$	$\mu_h = 360$	120	[16],
		$\mu_h = 2$	30	2017
EBIC/TMR	MWIR *n*B*p* InAs/GaSb	$\mu_e = 150$-200	80	**[23], 2019**
Magneto-Resistance (MSM)	MWIR *NID n*-type InAs/$InAs_{0.65}Sb_{0.35}$	$\mu_h = 3.73$	77	**[24],**
		$\mu_e = 4.4\times10^3$	77	**2019**
		$\mu_h = 11$	130	
		$\mu_e = 2.6\times10^3$	130	

IV. Publications and Presentations

"Carrier density and transport in Be-doped InAsSb for infrared detector materials", L. Casias, C. P. Morath, E. H. Steenbergen, P. Webster, J. Kim, V. Cowan, G. Balakrishnan, and S. Krishna, MIOMD, October 2018, Poster Presentation.

Casias, Lilian K., et al. "Carrier concentration and transport in Be-doped InAsSb for infrared sensing applications." Society of Photo-Optical Instrumentation Engineers (SPIE) Conference Series. Vol. 10624. 2018.

Casias, Lilian K., et al. "Carrier concentration and transport in Be-doped InAsSb for infrared sensing applications." Infrared Physics & Technology 96 (2019): 184-191.

Z. Taghipour et al., "Temperature-Dependent Minority-Carrier Mobility in p -Type InAs / GaSb Type-II Superlattice Photodetectors," Phys. Rev. Appl., vol. 11, no. 024047, 2019.

*** It must be noted that the magneto-transport work on MSM magneto-transport will include one or two future publications as the student just finished their PhD and getting articles ready for review.*

Dissertations:

Vertical Transport Study of III-V Type-II Superlattices, Zahra Taghipour, University of New Mexico, December 2018.

Transport in Mid-Wavelength Infrared (MWIR) p- and n- type InAsSb and InAs/InAsSb Type-II Strained Layer Superlattices (T2SLs) for infrared detection, Lilian K. Casias, University of New Mexico, May 2019

Bibliography

[1] W. S. A. Krier, "Uncooled photodetectors for the spectral range 3-5 μm based on III – V heterojunctions," *Appl. Phys. Lett.*, vol. 89, no. 083512, 2006.

[2] M. Carras, J. L. Reverchon, G. Marre, C. Renard, B. Vinter, and X. Marcadet, "Interface band gap engineering in InAsSb photodiodes," *Appl. Phys. Lett.*, vol. 87, no. 102103, 2005.

[3] G. A. Sai-Halasz, R. Tsu, and L. Esaki, "A new semiconductor superlattice," *IBM J. Res. Dev.*, 1977.

[4] D. L. Smith and C. Mailhiot, "Proposal for strained type II superlattice infrared detectors," *J. Appl. Phys.*, vol. 62, no. 6, pp. 2545–2548, 1987.

[5] C. Cervera *et al.*, "Transport measurements on InAs/GaSb superlattice structures for mid-infrared photodiode," *J. Phys. Conf. Ser.*, vol. 193, no. 001, p. 012030, 2009.

[6] G. a. Umana-Membreno *et al.*, "Electronic transport in InAs/GaSb type-II superlattices for long wavelength infrared focal plane array applications," *Spie*, vol. 8353, p. 83530Y–83530Y–5, 2012.

[7] Y. Lin, D. Wang, D. Donetsky, and G. Kipshidze, "Transport properties of holes in bulk InAsSb and performance of barrier long-wavelength infrared detectors," *Semicond. Sci. Technol.*, vol. 29, no. 112003, 2014.

[8] Y. Lin *et al.*, "Effect of hole transport on performance of infrared type-II superlattice light emitting diodes," *J. Appl. Phys.*, vol. 117, no. 16, pp. 1–5, 2015.

[9] D. Zuo *et al.*, "Direct minority carrier transport characterization of InAs/InAsSb superlattice nBn photodetectors," *Appl. Phys. Lett.*, vol. 106, no. 7, pp. 2–6, 2015.

[10] S. M. E.H. Steenbergen, S. Elhamri, W.C. Mitchel, "Carrier transport properties of Be-doped InAs / InAsSb type-II infrared superlattices," *Appl. Phys. Lett.*, vol. 104, no. 011104, 2014.

[11] J. W. McClure, "Field dependence of magnetoconductivity," *Phys. Rev.*, vol. 101, pp. 1642–1646, 1956.

[12] L. K. Casias *et al.*, "Infrared Physics & Technology Carrier concentration and transport in Be-doped InAsSb for infrared sensing applications," *Infrared Phys. Technol.*, vol. 96, no. July 2018, pp. 184–191, 2019.

[13] W. A. Beck and J. R. Anderson, "Determination of electrical transport properties using a novel magnetic field-dependent Hall technique," *J. Appl. Phys.*, vol. 62, no. 2, pp. 541–554, 1987.

[14] I. Vurgaftman *et al.*, "Improved quantitative mobility spectrum analysis for hall characterization," *J. Appl. Phys.*, vol. 84, no. 9, pp. 4966–4973, 1998.
[15] G. A. Umana-Membreno *et al.*, "Investigation of Multicarrier Transport in LPE-Grown Hg1-xCdxTe Layers," *J. Electron. Mater.*, vol. 39, no. 7, 2010.
[16] B. V. Olson *et al.*, "Vertical Hole Transport and Carrier Localization in InAs/InAs1−xSbx Type-II Superlattice Heterojunction Bipolar Transistors," *Phys. Rev. Appl.*, vol. 7, no. 024016, 2017.
[17] A. Brown, "Application of Mobility Spectrum Analysis to Modern Multi-layered IR Device Material," University of illinois at Chicago, 2015.
[18] N. Yoon, C. J. Reyner, G. Ariyawansa, J. E. Scheihing, J. Mabon, and D. Wasserman, "Diffusion Characterization of In (Ga) As / InAsSb Type-II Superlattices via Electron Beam Induced Current and Time- Resolved Photoluminescence," *2016 IEEE Photonics Conf.*, vol. 2, 2016.
[19] S. Suchalkin *et al.*, "In-plane and growth direction electron cyclotron effective mass in short period InAsGaSb semiconductor superlattices," *J. Appl. Phys.*, vol. 110, pp. 1–6, 2011.
[20] G. a. Umana-Membreno *et al.*, "Vertical minority carrier electron transport in p-type InAs/GaSb type-II superlattices," *Appl. Phys. Lett.*, vol. 101, pp. 1–5, 2012.
[21] B. V. Olson, L. M. Murray, J. P. Prineas, M. E. Flatt??, J. T. Olesberg, and T. F. Boggess, "All-optical measurement of vertical charge carrier transport in mid-wave infrared InAs/GaSb type-II superlattices," *Appl. Phys. Lett.*, vol. 102, pp. 1–5, 2013.
[22] Y. Lin, D. Wang, D. Donetsky, and G. Kipshidze, "Transport properties of holes in bulk InAsSb and performance of barrier long-wavelength infrared detectors," *Semicond. Sci. Technol.*, vol. 112002, no. 29, 2014.
[23] Z. Taghipour *et al.*, "Temperature-Dependent Minority-Carrier Mobility in p -Type InAs / GaSb Type-II-Superlattice Photodetectors," *Phys. Rev. Appl.*, vol. 11, no. 024047, 2019.

[24] Transport in Mid-Wavelength Infrared (MWIR) p- and n- type InAsSb and InAs/InAsSb Type-II Strained Layer Superlattices (T2SLs) for infrared detection, Lilian K. Casias, University of New Mexico, Dissertation, May 2019.